Impact of Wind Generators in Power System Stability

F. R. ISLAM, A. LALLU, K. A. MAMUN, K. PRAKASH AND A. A. RATTAN
School of Engineering and Physics, Faculty of Science and Technology
The University of the South Pacific
Laucala Bay, Suva
FIJI
islam_f@usp.ac.fj www.usp.ac.fj

Abstract: - Wind electricity is one of the quickest developing renewable resources of power. This rapid development is expected considering the environmental factors, but in terms of power system stability, it comes with a number of concerns. Generators play a vital role on stability for a particular capacity and design of a network. This paper investigated the overall performance of 3 foremost types of wind turbines via small signal stability analysis on IEEE 9 bus system. Simulations have been done and established that the generators dynamic model have significant impact on power system stability at different capacity of the generators.

Key-Words: - Wind Turbines, Signal Stability Analysis, Critical Parameter, Penetration Level, Grid Code, Eigenvalues

1 Introduction

Recently the penetration of wind energy in power network is increasing rapidly. In comparison to other sources of renewable energy, wind energy has significant importance with its remarkable advantages. In recent years, wind generators of different size have been installed in various part of the world. Increasing penetration of wind energy in to the existing power grid became a great concern in terms of control and dynamic stability of the systems.

Power systems stability problems develop through stressful operation conditions, increasing interconnections of new technologies and controls. Different forms of instability emerge in terms of voltage stability, frequency stability and angle stability which became an apprehension in the recent past [1]. The output power from wind energy conversion system (WECS) is prone to oscillate for the torsional characteristic of drive train and results in power system instability [2, 3].

The wind turbine generators (WTGs) are separated into two fundamentals configuration: fixed and variable speed. A squirrel cage induction generator (SCIG) is usually used as fixed-speed WTG while the permanent magnet synchronous generators (PMSGs) are popular for variable speed WTGs because of the wider range ability of capturing the energy from the different wind speed. It could deliver better power quality with a potential to adjust the power factor with the aid of generating reactive electricity. Similarly, doubly fed induction generators (DFIGs) also perform in variable-speed (constant frequency) system with an opportunity to control active and reactive power independently as the rotor speeds of a DFIG can be controlled from the generator side [4].

In DFIG, rotor is connected through back to back AC/DC/AC converters and the stator is connected directly to the grid. The control scheme of DFIG is decoupled with the rotor speed using the grid frequency [5]. Wind turbine is a combination of subsystems, i.e. drive train and generator. The available aerodynamic mechanical power is given as P_{ω} in (1). Betz Limit states, maximum 59.3% of wind power ($P_{\omega o}$) can be extracted through wind turbine [3], which is represented as (2).

$$P_{\omega} = \frac{1}{2}\rho A u^3 \quad (1)$$

$$P_{\omega o} = \frac{1}{2}\rho A C_p(\lambda, \beta) u^3 \quad (2)$$

Where A is cleared area of rotor blades, ρ is the air density, u is wind speed, β is the blade pitch angle and Cp is power coefficient. The tip speed ratio λ can be defined as (3).

$$\lambda = \frac{\omega_r R}{u} \quad (3)$$

Where the angular rotational speed of the rotor is ω_r and length of the rotor blade is R. The damping of the electromechanical modes in the oscillation is associated with the dynamic performance and small signal stability in the network. Whereas, the oscillatory behaviour is associated with the variation

in the electrical torques due to the changes in rotor angle and inertia [4].

The penetration of huge wind energy can change the damping presentation of whole system by alternating the power flows or the dispatch of the synchronous generation [6]. Consequently, the penetration level of renewable energy from wind generators have an effect on power system dynamic stability and reliability [7], which deals with frequency fluctuations, harmonics and economical dispatch of electricity [8-13]

Typically, the level of wind power penetration in the power system networks are on an average of 20-30 % and it could be even up to 100% [20]. As the penetration of wind energy upsurges into network, its impact is no longer limited to the distribution or transmission system but starts to influence the whole power network. An investigation on wind power penetration effect has been done in this research utilizing small signal stability investigation to think about the dynamic completion of the power systems. For this study, the Weibull distribution model which comprises turbulence, average wind speed, ramp and gust has been used. A low pass filter with time constant τ (as shown in Fig. 1) is being used to calculate high frequency wind speed which can be calculated using (4).

$$\frac{d}{dt}u_m = (\breve{u}_\omega(t) - u_\omega)/\tau \qquad (4)$$

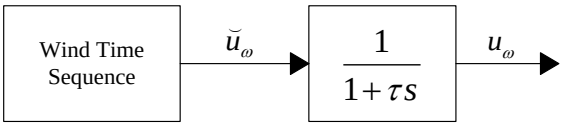

Fig. 1 Varying wind speed using Low-Pass Filter

To characterize and define the power loss from various wind turbines generators, simulation scenarios are outlined in [21]. However, this paper explores the stability of power system based on the wind energy penetration level for various types of generators using IEEE 9 bus system while maintaining the electrical grid code.

2 Grid Code

The electrical energy grid code is a legal and regulatory set of procedures that must be followed and accepted by when dealing with grid related operations like; designing, developing, sustaining and functioning the grid. Grid code deals with power control (active and reactive), high and low voltage trip through capability during system failure and disruption. Issues that have been intensive on grid networks are:

1. Operating range for frequency and voltage
2. Control of frequency, voltage with active and reactive power
3. Low and high voltage ride through (L/HVRT)
4. Power quality
5. Wind farm modeling and verification
6. Communications and external control

Grid code requirement states that wind farms must be capable to operate within the rated voltage and frequency variation limits faced in normal and outside operating conditions during energy generation. Wind generators must be designed suitably as unexpected frequencies usually overheats the generator winding; lower insulation material & damaging the power electronic devices [22].

3 Wind Energy Penetration Level

The level of wind energy penetration into the grid is not limited by any research till date according to the literature review but the grid engineers are expecting that there will be stability problem after a certain amount of penetration [23]. The penetration level is well-defined by percentage fraction of total load (P_{Load}) serve over wind energy power (P_{wg}) as in (5).

$$Penetration(\%) = (P_{wg} / P_{Load})x100\% \qquad (5)$$

Various level of penetration analysis through linearization-based eigenvalue examination, time area reenactments and probabilistic eigenvalue examination [15] demonstrate that vast wind energy combination can have positive or negative effects on framework damping.

3.1 WTGs Comparisons

WTGs have their own advantages and disadvantages as elaborated [8, 9, 11, 24] and summarized in Table 1 [32]. Many researches have claimed that different generator performed well in different environment [14-19]. The generators comparison in [31] outlined that SCIG has effects on the aggregated inertia of the power generation that lowers the overall torsional oscillating frequency in the system. PMSG provides added damping to some of the critical

modes of operation whenever energy created by wind is penetrated into the network of power system. DFIG in the power system is considered as a stable generator which has improved transient stability due to its converters and stability outputs. In addition, this generator has more control over SCIG in terms of reactive power and greater energy capture and is cheaper in cost as power electronics is rated at 30% of the DFIG rating rather than 100% in the case of PMSG.

Types	Advantages	Disadvantages
DFIG	Less noisy, efficient (aerodynamically), small rating converter	Less efficient (electrical), costly and gear box
SCIG	Cheaper, efficient (electrical), robust and simple structure	Low efficient (aero dynamical), noisy, higher mechanical stress, gear box
PMSG	Less noisy, efficient (aerodynamically), gearless, Low mechanical stress	Requires large rating converter, costly, heavy and bulky

Table 1 Comparisons for WTGs

4 Stability Analysis

Stability in Power System is characterized as the capacity for a specific working condition to recover a state of operational equilibrium where most system factors are enclosed, so essentially the entire system stays operational and in place [2]. In power system [30], minority of the signal stability is influenced by the elements which incorporate initial operating conditions, quality of electrical connections among components, characteristics of the different control tools and so on. Further verification on the stability based on the penetration level (different types of WECS) is discussed later in this paper. The analysis of the critical parameters in the power system will lead to proper planning management and designing of the network for penetrating wind power into the network.

4.1 Small-Signal Stability

Small-Signal Stability is the capability in power system network to transits into a stable functional or operational point or to the defined steady state caters for the event of a fault that leads to the variations in the state variables of the network [25] and can be expressed using (6) and (7).

$$(d/dt)x = A(d/dt)x + B(d/dt)f \quad (6)$$

$$(d/dt)y = C(d/dt)x + D(d/dt)f \quad (7)$$

Where, *(d/dt)x* is the derivative of state vector, the input vector *(d/dt)f*, the output vector *(d/dt)y*, *A* is the state matrix, *B* is the input matrix, *C* is the output matrix and *D* is the feed-forward. Finally, (8) is being used to represent the state space equation of the system linearized model.

$$(d/dt)x = A(d/dt)x \quad (8)$$

If power system produces oscillations caused by small disturbances which can be suppressed, such that the deviations of the system state variables may remain small for a long period, thus the power system is considered stable. On the contrary, if the magnitude of the oscillation continues to gain or increase indefinitely, the power system becomes unstable. However, because it is inevitable, the power system which is unstable in terms of the small signal stability concept cannot operate in practical.

The following condition can determine stability of the a system [32], which helps to understand and study about the stability of a nonlinear system at an operating point,

- Linearized system is asymptotically stable, i.e., all eigenvalues have negative real part and are globally stable at equilibrium point.
- Linearized system is unstable, i.e., at least one Eigen values of a has positive real part and is unstable at equilibrium point.
- Linearized system is critically stable. i.e., real parts of all eigenvalues are negative but real part of the point has at least one of them at zero, therefore, no conclusion can be drawn about the stability.

4.2 Eigen Value

The stability of a linearized system is defined by the eigenvalues in the state matrix. The conjugate pair eigenvalue indicating oscillatory mode for the response in real and imaginary part can be expressed using (9).

$$\lambda = \sigma + j\omega \quad (9)$$

For a pair of conjugate eigenvalues that are made of complex numbers and each pair corresponds to an

oscillatory mode, where λ is the eigenvalue, σ is the damping coefficient and $j\omega$ is the damped natural frequency [27],where a negative complex eigenvalues, represents a damped system. The damping ratio (ζ) can be expressed as (10).

$$\zeta = -\sigma / \sqrt{\sigma^2 + \omega^2} \tag{10}$$

The system becomes unstable if ζ is negative. Hence to ensure that there is an acceptable performance, a damping ratio margin is placed in the range of 3% to 5% [28], if all the electromechanical modes have been adequately considered. The three types of generators impact from damping is shown in Table 2.

Types	Positive	Negative
DFIG	✔	✔
SCIG	✔	
PMSG	✔	✔

Table 2 Possible Effects of WTGs on Damping

5 Modeling of Constant Wind Speed Turbine

5.1 Modeling of DFIG

In this research, DFIG state space equations [29] have been used. Table A.1, in Appendix shows the details parameter of DFIG used for the analysis and Fig. 2 illustrates the model of DFIG.

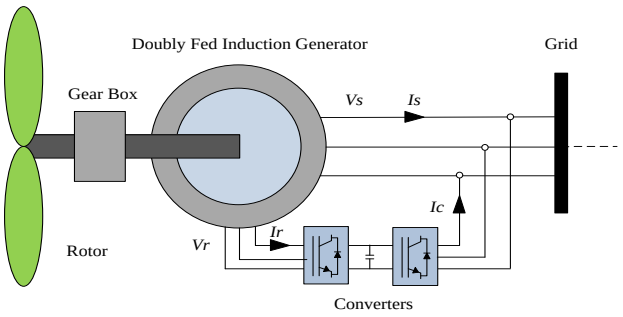

Fig. 2 Model diagram for DFIG

The representation of stator voltage are the functions derived from the voltage magnitude and the phase angle in the d-axis (v_{ds}) as direct stator voltage and q-axis (v_{qs}) as quadrature stator voltage can be expressed as (11) and (12) respectively.

$$v_{ds} = V \sin(-\theta) \tag{11}$$

$$v_{qs} = V \cos(-\theta) \tag{12}$$

It is significant to note that the active power P_D and reactive power Q_D, which are included in the grid depending on the current from the stator and current from the converters from the grid side current as shown in (13) and (14) where, i_{ds} is direct stator current, i_{qs} is the quadrature stator current and i_{qc} is the quadrature current.

$$P_D = v_{ds} i_{ds} + v_{qs} i_{qs} + v_{dc} i_{dc} + v_{qc} i_{qc} \tag{13}$$

$$Q_D = v_{qs} i_{ds} + v_{ds} i_{qs} + v_{qc} i_{dc} + v_{dc} i_{qc} \tag{14}$$

The electrical torque T_{eD} and mechanical torque T_{mD} are given by (15) and (16) respectively.

$$T_{eD} = x_m (i_{qr} i_{ds} - i_{dr} i_{qs}) \tag{15}$$

$$T_{mD} = P_w / \omega_m \tag{16}$$

5.2 SCIG Modeling

The SCIG model is illustrated in Fig. 3 and the state space electrical equations were used will be found in [29]. Table A.2, in Appendix shows the details parameter of SCIG used for the analysis.

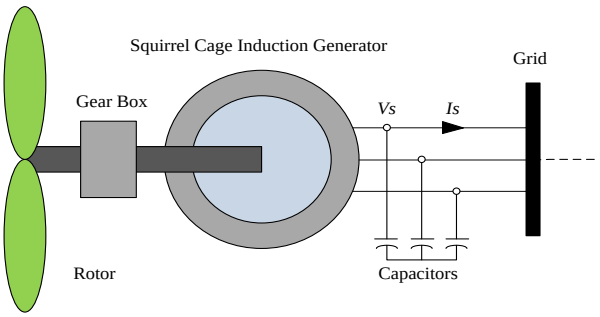

Fig. 3 Model diagram for SCIG

The network voltage can be represented in the real (v_r) axis and imaginary (v_m) axis of the stator machine and is expressed using (17) and (18).

$$v_r = V \sin(-\theta) \tag{17}$$

$$v_m = V \cos(-\theta) \tag{18}$$

Power absorption equations are given as active (P_s) in (19) and reactive (Q_s) in (20) where v_r and i_r are the real voltage and current, v_m and i_m is the

imaginary voltage and current and b_c is the fixed capacitor conductance.

$$P_s = v_r i_r + v_m i_m \quad (19)$$

$$Q_s = v_m i_r - v_r i_m + b_c(v_r{}^2 + v_m{}^2) \quad (20)$$

The electrical torque T_{eS} and the mechanical torque T_{tS} are given by (21) and (22) where, e'_r and i_r is the real part of 1st cage voltage and current and e'_m and i_m is the imaginary of 1st cage voltage and current. The mechanical torque (SCIG) is represented as T_{tS}.

$$T_{eS} = e'_r i_r + e'_m i_m \quad (21)$$

$$T_{tS} = P_\omega / \omega_t \quad (22)$$

The mechanical dynamic equations which incorporate the turbine inertia (H_t) and rotor (H_m) and shaft stiffness (K_s) are defined using (23), (24) and (25) and the link between state variables, current and voltage are defined in (36) and (37). Where ω_{tS} is the wind turbine angular speed, ω_{mS} is the rotor angular speed, γ is the relative angle displacement, Ω_b as the system rated frequency and x_0 and x' are the initial and 1st reactance value respectively.

$$(d/dt)\omega_{tS} = (T_{\omega r} - K_s\gamma)/(2H_t) \quad (23)$$

$$(d/dt)\omega_{mS} = (K_s\gamma - T_e)/(2H_m) \quad (24)$$

$$(d/dt)\gamma = \Omega_b(\omega_t - \omega_m) \quad (25)$$

$$(d/dt)e'_r = \Omega_b(1-\omega_m)e'_m - \left(e'_r - (x_0 - x')i_m\right)/T_0' \quad (26)$$

$$(d/dt)e'_m = -\Omega_b(1-\omega_m)e'_r - \left(e'_m + (x_0 - x')i_r\right)/T_0' \quad (27)$$

5.3 PMSG Modeling

Permanent magnet synchronous generator state space electrical equation which will be found in [29] is illustrated in Fig. 4. Table A.3, in Appendix shows the details parameter of PMSG used for the analysis.

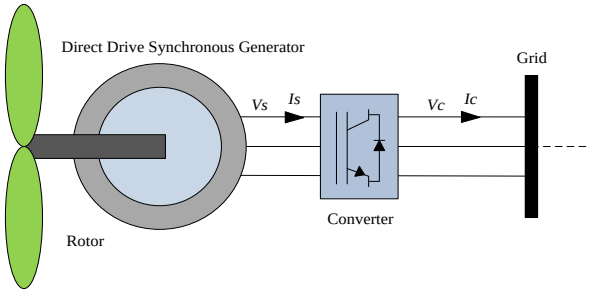

Fig. 4 Model diagram for PMSG

The rotor and stator flux dynamic voltage equations and represented in (28) and (29).

$$v_{ds} = -r_s i_{ds} + \omega_m x_q i_{qs} \quad (28)$$

$$v_{qs} = -r_s i_{qs} - \omega_m(x_q i_{ds} - \psi_p) \quad (29)$$

The active and reactive powers of the generator are represented in (30) and (31) respectively.

$$P_{sP} = v_{ds} i_{ds} + v_{qs} i_{qs} \quad (30)$$

$$Q_{sP} = v_{qs} i_{ds} - v_{ds} i_{qs} \quad (31)$$

The active and reactive power that is input into the grid depends on the grid side current of the converter according to (32) and (33).

$$P_{cP} = v_{dc} i_{dc} + v_{qc} i_{qc} \quad (32)$$

$$Q_{cP} = v_{qc} i_{dc} - v_{dc} i_{qc} \quad (33)$$

The voltages from converter are the represented by the grid voltage magnitude and phase angle as shown in (34) and (35):

$$v_{dc} = V\sin(-\theta) \quad (34)$$

$$v_{qc} = V\cos(-\theta) \quad (35)$$

The dynamic equation of the rotor speed (ω_{mP}) is demonstrated using (36). The ideal current source is derived from by the converter, where i_{qs}, i_{ds} and i_{dc} are state variables expressed using as (37), (38) and (39) respectively. For PMSG the variables are, T_m as the mechanical torque, T_e as the electrical torque, i_{dsref} and i_{qref} as the direct and quadrature stator reference current respectively, T_{eP} as the active power control time constant, K_v as the coefficient of the voltage time derivative and T_v as the voltage control time constant.

$$(d/dt)\,\omega_{mP} = (T_m - T_e)/(2H_m) \quad (36)$$

$$(d/dt)i_{ds} = \left(i_{dsref} - i_{ds}\right)/T_{\in p} \quad (37)$$

$$(d/dt)i_{qs} = \left(i_{qsref} - i_{qs}\right)/T_{\in p} \quad (38)$$

$$(d/dt)i_{dc} = (K_V(V_{ref} - V) - i_{dc})/T_V \quad (39)$$

5.4 Synchronous Machine (SM)

The SM has a lead-lag transfer function which is used to model (shown in Fig. 5). A fourth order system with state variables (δ, ω, e'_q and e'_d) has been considered in this research which can be expressed by (40)-(43). Where δ_{SM} is the machine rotor angle, ω_{SM} is the angular frequency, p_m is the mechanical power and p_e is the electrical power, x_d is the d-axis synchronous reactance, x'_d is the d-axis transient reactance, υ^*_f is the feedback field voltage, e'_q constant amplitude e.m.f. e'_q, e'_d subtransient d-axis voltage, T'_{d0} is the d-axis open circuit transient time constant and T'_{q0} is the q-axis open circuit transient time constant.

$$(d/dt)\delta_{SM} = \Omega_b(\omega_{SM} - 1) \quad (40)$$

$$(d/dt)\omega = (p_m - p_e - D(\omega - 1))/M \quad (41)$$

$$(d/dt)e'_q = (-f_s(e'_q) - (x_d - x'_d)i_d + \upsilon^*_f)/T'_{d0} \quad (42)$$

$$(d/dt)e'_d = (-e'_d + (x_q - x'_q)i_q)/T'_{q0} \quad (43)$$

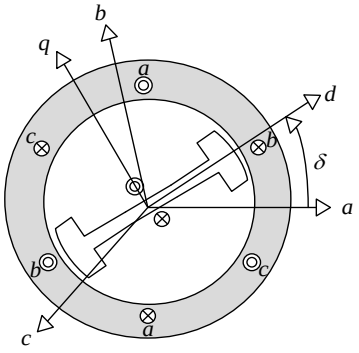

Fig. 5 Synchronous machine scheme [25]

5.5 Automatic Voltage Regulator (AVR)

Standard type II AVR has been used for this study which is a standard IEEE AVR model 1 is described using the equations (44) – (47). Where, V_m is the voltage signal, T_r is the time constant, V_{ref} is the reference voltage, K_f is the gain of the stabilizer, T_f is time constant of stabilizer, V_f is the field voltage, V_{r1} is amplifier state variable 1, V_{r2} is amplifier state variable 2, S_e is the ceiling function coefficient and T_e is the field circuit time constant.

$$(d/dt)V_m = (V - V_m)/T_r \quad (44)$$

$$(d/dt)V_{r1} = (K_a(V_{ref} - V_m - V_{r2} - (K_f/T_f)V_f) - V_{r1})/T_r \quad (45)$$

$$V_r = \begin{cases} V_{r1} & if....V_{r\min} \le V_{r1} \le V_{r\max}, \\ V_{r\max} & if....V_{r1} > V_{r\max}, \\ V_{r\min} & if....V_{r1} < V_{r\min}, \end{cases}$$

$$(d/dt)V_{r2} = -((K_f/T_f)V_f + V_{r2})/T_f \quad (46)$$

$$(d/dt)V_f = -(V_f(1 + S_e(V_f)) - V_r)/T_e \quad (47)$$

6 Test System Description

A modified IEEE 9 bus network with three area and two machines system has been used for this research as shown in Fig. 6. Where a synchronous machine is connected on bus 2, a slack bus on bus 1 and DFIG/SCIG/PMSG has been replaced one by one to bus 3 to identify the stability with different scenario using the parameters shown in Table 3. For each case, wind orientation, power flow and time domain analysis have been carried out. The wind turbine generator capacity has been varied from 0.2MW to 3MW. Grid code is ensured for the system to produce optimal power at 30% wind power penetration while the SM and the slack bus were adjusted accordingly. The AVR has been used as a regulator and a comparative analysis using eigenvalues plots to determine the stability.

System Characteristics	Value
No. of buses	9
No. of generators	4
No. of transmissions	6
Total Gen. Power	9MW
Types of Gen.	DFIG/SCIG/ PMSG & SG
Total Load	9MW

Table 3 Parameters of the Distributed Network

Using (5) the penetration levels have been set up to 33.33% for penetration of Distributed Generator (DG). The parameters of the IEEE 9 bus system is given in Table 4. 0, in Appendix shows the details parameter of IEEE 9 bus system used for the analysis and the base value has been given in Appendix Table A.5.

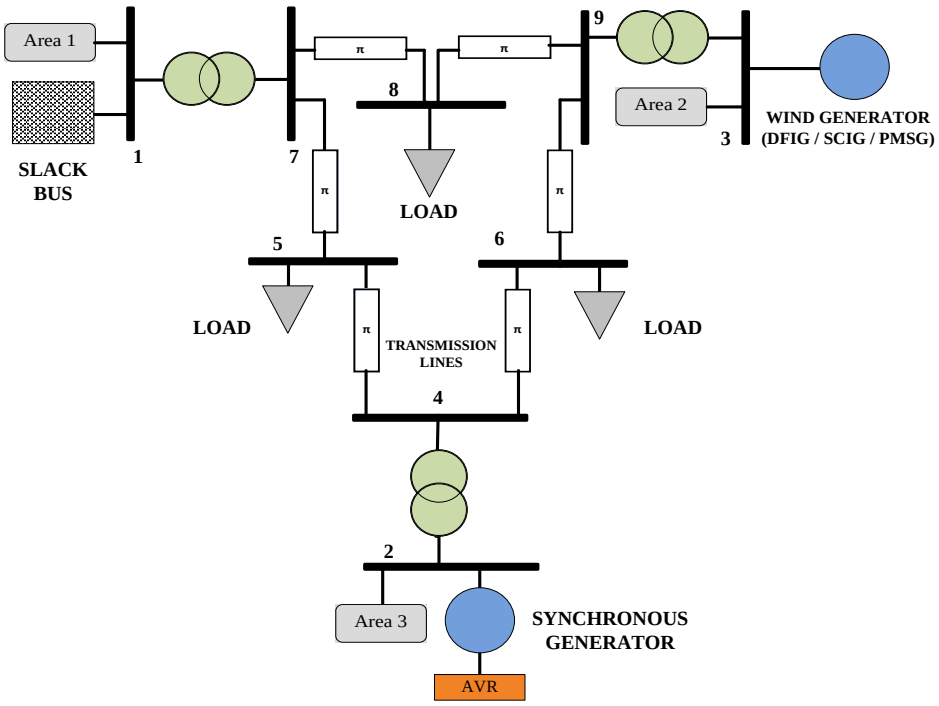

Fig. 6 The IEEE 9 Bus 3 area system with various wind generators connection at bus no.3

Wind Turbine	Synchronous Generator	Bus 1, 2, 3	Bus 4, 5, 6, 7, 8, 9
11KV, 60Hz	11KV, 60Hz	11KV	33KV

Table 4 Parameters of Network with DFIG, SCIG & PMSG

7 Associate Control Systems

Similar control techniques have been used to control rotor speed, voltage and pitch angle for all the cases. Converter is modeled for rotor speed control as shown in Fig. 7 and the voltage control as shown in Fig. 8. P^*_{ω} (ω_m) is the characteristic which approximately enhances the wind energy capture calculated from speed. The use of anti-windup limiters avoids converter over-speed during the speed and voltage control. By assuming bus voltage $V \approx 1$ to calculate rotor current limits. The pitch angle to θ_p=0 for anti-windup limiter has been locked for sub-synchronous speeds as shown in Fig. 9.

The converter dynamics are highly simplified with respect to electromechanical transients, the ideal currents sources where i_{qs} and i_{dr} are state variables and are used for rotor speed and voltage control respectively which are defined as (48) and (49). The pitch angle control is defined in (50). Where, $-x_s$ is the stator reactance, $-x_m$ is the magnetizing reactance, P^*_w is the power speed characteristics, T_ϵ is the power control time constant, K_v is the coefficient of the voltage time derivative, K_p is the active power feedback gain, φ is the transformer phase shift and Θ_p is the angular position.

$$(d/dt)i_{qr} = \left(\left(\left(-x_s + x_m\right)/x_m V\right)P^*_{\omega}\left(\omega_m\right)\right)/\omega_m - i_{qr}\Big)1/T_{\epsilon} \quad (48)$$

$$(d/dt)i_{dr} = K_V\left(V - V_{ref}\right) - V/x_m - i_{dr} \quad (49)$$

$$(d/dt)\theta_p = \left(K_p \varnothing\left(\omega_m - \omega_{ref}\right) - \theta_p\right)/T_P \quad (50)$$

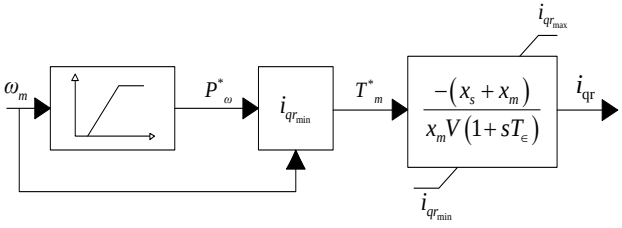

Fig. 7 Rotor speed control scheme

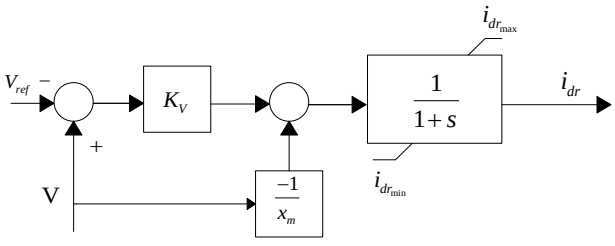

Fig. 8 Voltage control scheme

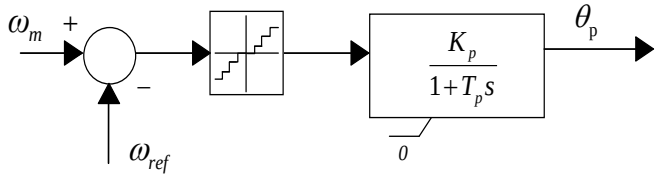

Fig. 9 Pitch angle control scheme

8 Small Signal Stability Analysis (SSSA)

Three levels of penetrations (≈9%, ≈20% and ≈33%) have been considered to explain how the generator behaves during the simulation of the network.

8.1 Doubly Fed Induction Generator

The DFIG model as shown in Fig. 2 has been used to penetrate power into the grid during the simulation. Up to 33.33% of wind energy penetration from DFIG, small signal stability has been analyzed and found stable. Table 5 summarized the data for various state variables at different penetration level. In this case, all the magnitudes of the frequency represent a stable system. The simulation analyses of the system are shown in Fig. 10 at 33.33% wind energy penetration from DFIG.

Eig	States	DFIG 9%	DFIG 20%	DFIG 33%
1	ω_m	-130.058	-124.6325	-1.2846
2	i_{dr}	-4.2743	-1.8753	-91.9102
3	i_{dr}	-1	-1	-128.8484
4	δ	-1	-1	-1
5	ω	-1	-1	-1
6	e'_q	-1	-1	-1
7	e'_d	-1000	-1000	-1
8	v_m	-5	-5	-1000
9	v_{r1}	-2.8571	-2.8571	-5
10	v_{r2}	-3.1971	-3.1971	-2.8571
11	v_f	-0.25	-0.25	-3.1971
12	v_m	-0.33333	-0.33333	-0.25
13	ϑ_p	-100	-100	-0.33333

Table 5 State Matrix Eigenvalues for DFIG

From the initial wind generator capacity of 0.2 MW, it is has been observed that the system maintained stability upto 3.0 MW. A consistent stable performance is observed from the 9 bus distribution network with DFIG.

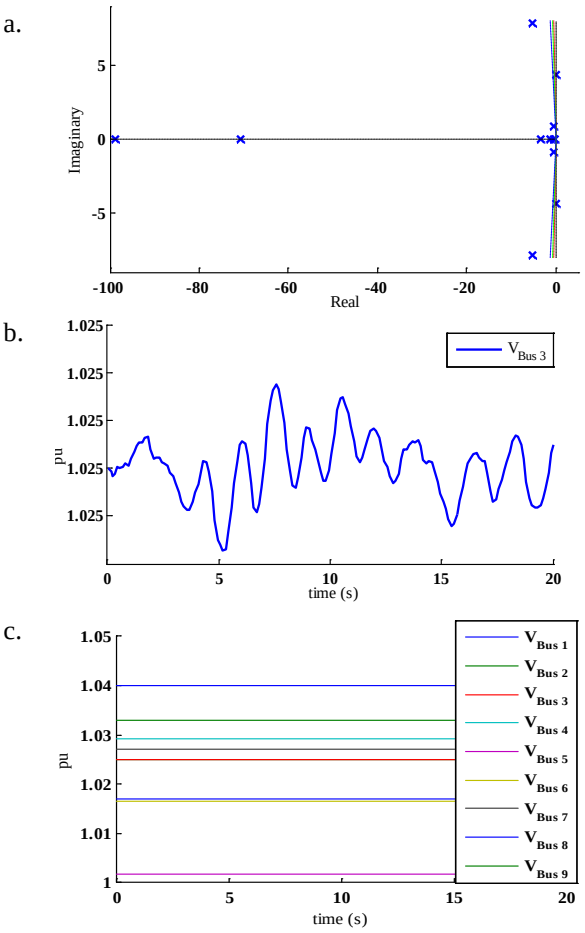

Fig. 10 Stable system at penetration level 33.33% for DFIG as in Table 5. (a) Eigenvalues Stability Plot, (b) Bus 3 Voltages at the DFIG generator and (c) 9 Buses Voltages

It is observed that the grid code stipulates that the maximum wind power output is harvested around 33% of wind power penetration for low level. The system stability can be authenticated via the eigenvalue plot analysis that has been carried out on each increment. Upon power flow analysis, the power system with DFIG portrayed stable operation by producing negative eigenvalues (poles) in the eigen plot. Bus voltages of all nine buses were plotted upon time domain analysis where Bus 3 is emphasized by connecting the DFIG wind turbine for penetrating wind power till 33% of wind power. The state values from the dynamic equations were ranging from marginal stability to stable performances.

8.2 Squirrel Cage Induction Generator

SCIG model as shown in Fig. 3 has been used to penetrate wind power into the network. Based on SSSA, the eigenvalues results show positive real eigenvalue which gives the poor damping. This shows that the system has imbalance performance characteristics at low level of wind energy penetration. Other levels of wind penetration data have been summarized in Table 6 for various state variables at different penetration level.

Eig	States	SCIG 9%	SCIG 20%	SCIG 33%
1	ω_m e'_r	-14.89+32.44	-5.19+31.46	-3.42+28.26
2	e'_m	-14.89-32.44	-5.19-31.46	-3.42-28.26
3	ω_t, γ	7.53	-3.79	-3.93
4	ω_t, γ	-0.30+4.37	-1.24+4.37	-0.85+4.14
5	δ	-0.30-4.368	-1.24-4.37	-0.85-4.14
6	ω	-1	-1	-1
7	e'_q	-1	-1	-1
8	e'_d	-1	-1	-1
9	υ_m	-1	-1	-1
10	υ_{r1}	-1000	-1000	-1000
11	υ_{r2}	-5	-5	-5
12	υ_f	-2.8571	-2.8571	-2.8571
13	υ_m	-3.1971	-3.1971	-3.1971
14	υ_m	-0.25	-0.25	-0.25

Table 6 State matrix Eigenvalues for SCIG

Inconsistent performance of stability in the network is observed in the distribution network. Upto ≈9% of wind power injection into the 9 buses, the generator could not stabilize leading to faults and instability with the generator's imaginary axis voltages and current linkages (e'_m).

a.

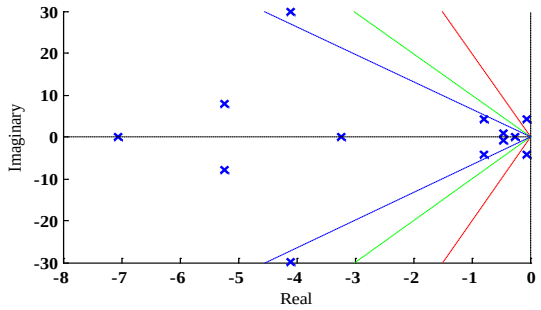

b.

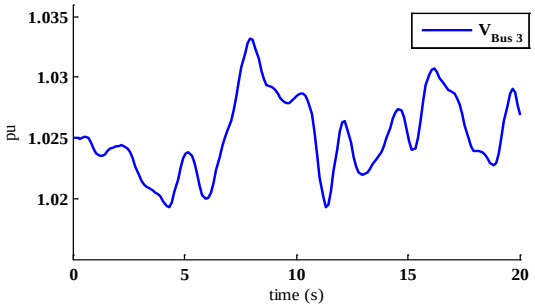

c.

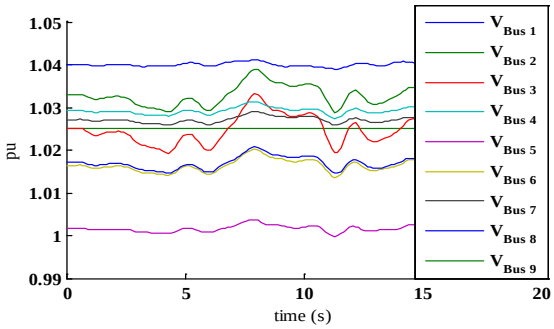

Fig. 11 Marginal stable system for penetration level up to 33.33% for SCIG as in Table 6. (a) Eigenvalues Stability Plot, (b) Bus 3 Voltages at the SCIG generator and (c) 9 Buses Voltages

The network has been verified from Fig. 11 eigenvalue plot, generator bus voltage and the 9 buses around the network to show the stability of system around 33% wind energy penetration using SCIG. The eigenvalues plot illustrates positive eigenvalues state variables. From the early stages of wind penetration, the network and wind generator is not performing well. However, with increasing wind penetration, the network showed that SCIG generator characteristics improved and remained marginal stable while producing wind power for the loads.

8.3 Permanent Magnet Synchronous Generator

PMSG model as shown in Fig. 4 is used to penetrate power into the grid. From the SSSA, the eigenvalues shows that the system stability varies in different level of penetration. The grid yields instability and oscillatory modes because of poor damping and unstable frequency of oscillation characteristic from the generator to penetrate up to 33% of wind power. The graphical analysis (Fig. 12) shows the instability of the system under 33% wind energy penetration using PMSG. Other levels of wind penetration data have been summarized in Table 7.

Eig	States	PMSG 9%	PMSG 20%	PMSG 33%
1	i_{dc}	-1	-1	-145.4421
2	ω_m	-1	-1	-0.58687
3	i_{qs}	-1	-1	43.451
4	δ	-1	-1	-1
5	ω	-1000	-1000	-1
6	e'_q	-5	-5	-1
7	e'_d	-2.8571	-2.8571	-1
8	v_m	-3.1971	-3.1971	-1000
9	v_{r1}	-3.1983	-132.0987	-5
10	v_{r2}	-0.25	-1.8028	-2.8571
11	v_f	-0.33333	-0.25	-3.1971
12	v_m	-100	-0.33333	-0.25
13	ϑ_p	-1	-100	-0.33333

Table 7 State matrix Eigenvalues for PMSG

A fluctuating behavior of stability is observed for the generator while in creating the wind penetration towards 30% of wind power in the grid. At different percentage penetration, this generator has issues with quadrature stator current (i_{qs}) instability causing faults in the power system generating positive eigenvalues as shown in Fig. 12 a.

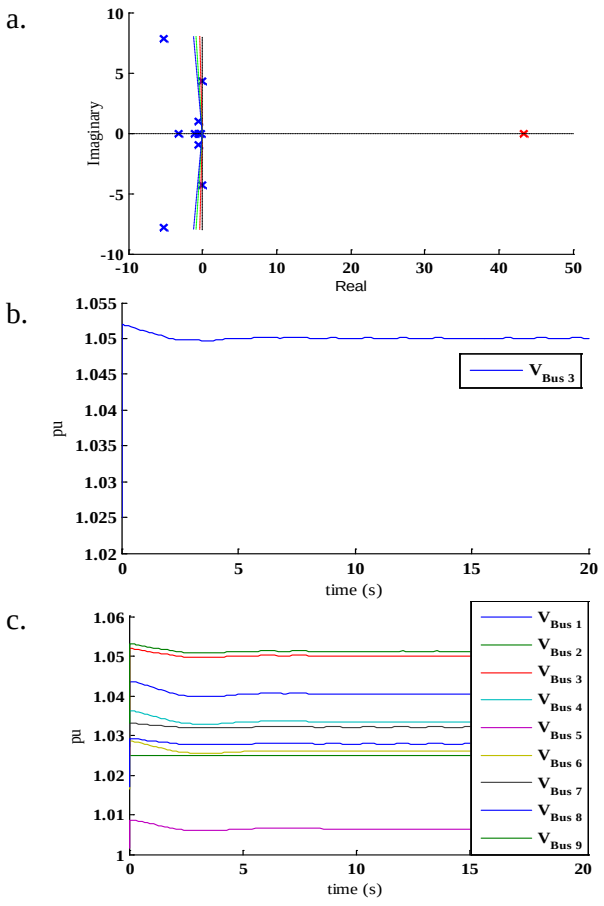

Fig. 12 Unstable system is at penetration level 33.33% for PMSG in accordance's to Table 7. (a) Eigenvalues Stability Plot, (b) Bus 3 Voltages at the SCIG generator and (c) 9 Buses Voltages

8.4 Impact of Penetration Level

This network analysis with the PMSG model yields unbalance characteristic of wind power penetration in the later (28%>) stages. Due to very little penetration dominance and its configuration of generator, PMSG becomes instable unpredictably. Considering that reactive power is essentially in the system, this power needs to be balanced against real power and leading to poor power factor ratio as PMSG do not require reactive for power generation.

DFIG (MVA)	SCIG (MVA)	PMSG (MVA)	PW (%)	Sync. Mach. (MVA)	Slack (MVA)
0.2	0.2*	0.2	2.22	4.4	4.4
0.4	0.4*	0.4	4.44	4.3	4.3
0.6	0.6	0.6	6.67	4.2	4.2
0.8	0.8*	0.8	8.89	4.1	4.1
1.0	1.0	1.0	11.11	4.0	4.0
1.2	1.2	1.2	13.33	3.9	3.9
1.4	1.4	1.4	15.56	3.8	3.8
1.6	1.6	1.6	17.78	3.7	3.7
1.8	1.8	1.8	20.00	3.6	3.6
2.0	2.0	2.0	22.22	3.5	3.5
2.2	2.2	2.2	24.40	3.4	3.4
2.4	2.4	2.4	26.67	3.3	3.3
2.6	2.6	2.6	28.89	3.2	3.2
2.8	2.8	2.8*	31.11	3.1	3.1
3.0	3.0	3.0*	33.33	3.0	3.0

* Unstable system with generator penetration level

Table 8 Stability Analysis for different penetration level scenarios

This SSSA table summary depicts that DFIG is more stable at a penetration level up to 33%. The impact analysis of penetration from the wind generator into the grid show different state variable performances and characteristic behaviors which yield stability matching the grid code for the network. Overall, DFIG had no issues in the generator configuration such as rotor angle, voltage and frequency stability in the grid. Critical parameters at the unstable mode are explained in Table 9.

Percentage (MVA)	SCIG	PMSG
2.22% (0.2)	ω_m, e'_r	
8.89% (0.6)	e'_m	
31.11% (2.8)		e'_q
33.33% (3.0)		i_{qs}

Table 9 Critical Parameters at the Unstable Mode for Generation Penetration

From the eigenvalues in Table 9, it can be concluded that the network has unstable state variables for frequency oscillations, voltage and current floatation in the generator. The critical parameters in Table II show that the states e'_r, ω_m, e'_m, e'_q and i_{qs} have the highest contribution in instability which implies that there are angle instability and voltage instability in the system.

9 Conclusion

This research study showed that the wind turbines have great amount of influencing factors for the small signal stability in the power system on its frequency and damping ratio. Penetration of large amounts wind energy in the network has the capabilities to alter the electromechanical performance of the network. For the stability analysis, Eigen values are computed from power flow equations by computing right and left eigenvectors of a Jacobian matrix. For SCIG, both normal and fault operation conditions require reactive power from the grid because it is operated with a fixed capacitor. Thus, SCIG instable performances such as over-speed and network instability are caused by power fluctuations. For PMSG, steady-state performance depends on the accuracy of calculating the synchronous reactance in the d-axes and q-axes. Also the instability occurs on the speed of the rotor due to the dependency on output voltage on the rotation speed. It can be concluded that at low penetration of the wind turbine generator, the whole grid becomes unstable for the SCIG. This study showed that low penetration of the wind turbine causes instability for the whole system where both machine's damped oscillation frequencies are is not locally in the stability mode. In addition, the PMSG becomes unstable for end range of the low penetration level around 33%. Simulation results conclude that SCIG and PMSG based systems is critical to be stable throughout in the IEEE 9 distribution network, whereas, DFIG is more predominant in remaining stable. This instability by SCIG and PMSG can be due to the reactive load characteristic and large amount of impedance in the grid producing poor power factor. Where, DFIG consist of power electronic devices, this makes a suitable technical solution to deliver wind power generation with power system control abilities and to enhance their effect on power system stability.

References:

[1] Kundur, P., Paserba, J., Ajjarapu, V., Andersson, G., Bose, A., Canizares, C., ... & Van Cutsem, T. (2004). Definition and classification of power system stability IEEE/CIGRE joint task force on stability terms and definitions. IEEE transactions on Power Systems, 19(3), 1387-1401.

[2] Tsourakis, G., Nomikos, B. M., & Vournas, C. D. (2009). Contribution of doubly fed wind generators to oscillation damping. IEEE Transactions on energy conversion, 24(3), 783-791.

[3] Jeevajothi, R. (2014). Impact Of Wind Turbine Generators On Power System Stability (Doctoral dissertation, Kalasalingam University).

[4] Sun, T., Chen, Z., & Blaabjerg, F. (2005). Flicker study on variable speed wind turbines with doubly fed induction generators. IEEE Transactions on Energy Conversion, 20(4), 896-905.

[5] Mehta, B., Bhatt, P., & Pandya, V. (2014). Small signal stability analysis of power systems with DFIG based wind power penetration. International Journal of Electrical Power & Energy Systems, 58, 64-74.

[6] Vowles, D. J., Samarasinghe, C., Gibbard, M. J., & Ancell, G. (2008, July). Effect of wind generation on small-signal stability—A New Zealand example. In Power and Energy Society General Meeting-Conversion and Delivery of Electrical Energy in the 21st Century, 2008 IEEE (pp. 1-8). IEEE.

[7] Sorensen, P., Cutululis, N. A., Vigueras-Rodríguez, A., Jensen, L. E., Hjerrild, J., Donovan, M. H., & Madsen, H. (2007). Power fluctuations from large wind farms. IEEE Transactions on Power Systems, 22(3), 958-965.

[8] Sun, Y., Wang, L., Li, G., & Lin, J. (2010, October). A review on analysis and control of

small signal stability of power systems with large scale integration of wind power. In Power System Technology (POWERCON), 2010 International Conference on (pp. 1-6). IEEE.

[9] Weisser, D., & Garcia, R. S. (2005). Instantaneous wind energy penetration in isolated electricity grids: concepts and review. *Renewable Energy*, *30*(8), 1299-1308.

[10] Slootweg, J. G., & Kling, W. L. (2003). The impact of large scale wind power generation on power system oscillations. Electric Power Systems Research, 67(1), 9-20.

[11] Mishra, Y. (2008). Advances in power system small signal stability analysis considering load modeling and emerging generation resource.

[12] Ekanayake, J. B., Holdsworth, L., Wu, X., & Jenkins, N. (2003). Dynamic modeling of doubly fed induction generator wind turbines. IEEE transactions on power systems, 18(2), 803-809.

[13] Ibrahim, H., Ghandour, M., Dimitrova, M., Ilinca, A., &Perron, J. (2011). Integration of wind energy into electricity systems: technical challenges and actual solutions. *Energy Procedia*, *6*, 815-824.

[14] Hagstrøm, E., Norheim, I., & Uhlen, K. (2005). Large-scale wind power integration in Norway and impact on damping in the Nordic grid. Wind Energy, 8(3), 375-384.

[15] Morshed, M. J., &Fekih, A. (2017). A new fault ride-through control for DFIG-based wind energy systems. *Electric Power Systems Research*, *146*, 258-269.

[16] Tsourakis, G., Nomikos, B. M., & Vournas, C. D. (2009). Effect of wind parks with doubly fed asynchronous generators on small-signal stability. Electric Power Systems Research, 79(1), 190-200.

[17] Zheng, C., &Kezunovic, M. (2012). Impact of wind generation uncertainty on power system small disturbance voltage stability: A PCM-based approach. *Electric Power Systems Research*, *84*(1), 10-19.

[18] Islam, F. R., & Pota, H. R. (2013). V2G technology to design a smart active filter for solar power system. International Journal of Power Electronics and Drive Systems, 3(1), 17.

[19] Islam, F. R., & Pota, H. R. (2011, November). V2G technology to improve wind power quality and stability. In Australian Control Conference (AUCC), 2011 (pp. 452-457). IEEE.

[20] Chen, Z. (2005). Issues of connecting wind farms into power systems. In Transmission and Distribution Conference and Exhibition: Asia and Pacific, 2005 IEEE/PES (pp. 1-6). IEEE.

[21] González-Longatt, F. M. (2007, October). Impact of distributed generation over power losses on distribution system. In 9th International Conference on Electrical Power Quality and Utilization.

[22] Sourkounis, C., & Tourou, P. (2013, June). Grid code requirements for wind power integration in europe. In Conference Papers in Science (Vol. 2013). Hindawi Publishing Corporation.

[23] Enslin, J. (2009). Grid impacts and solutions of renewables at high penetration levels. Quanta Technology.

[24] Herbert, G. J., Iniyan, S., Sreevalsan, E., & Rajapandian, S. (2007). A review of wind energy technologies. Renewable and sustainable energy Reviews, 11(6), 1117-1145.

[25] López, Y. U., & Domínguez, J. A. (2015). Small Signal Stability Analysis of Wind Turbines.

[26] Wilch, M., Pappala, V. S., Singh, S. N., & Erlich, I. (2007, July). Reactive power generation by DFIG based wind farms with AC grid connection. In Power Tech, 2007 IEEE Lausanne (pp. 626-632). IEEE.

[27] Nouby, M., Mathivanan, D., & Srinivasan, K. (2009). A combined approach of complex eigenvalue analysis and design of experiments (DOE) to study disc brake squeal. International Journal of Engineering, Science and Technology, 1(1), 254-271.

[28] Ruhle, O. (2006). Eigenvalue Analysis – All Information on Power System Oscillation. Behavior Rapidly Analyzed (1st ed.). Siemens PTI.

[29] Milano, F. (2010). *Power system modelling and scripting*. Springer Science & Business Media.

[30] Lee, D. J., & Wang, L. (2008). Small-signal stability analysis of an autonomous hybrid renewable energy power generation/energy storage system part I: Time-domain simulations. IEEE Transactions on Energy Conversion, 23(1), 311-320.

[31] Kong, S. Y., Bansal, R. C., & Dong, Z. Y. (2012). Comparative small-signal stability analyses of PMSG-, DFIG-and SCIG-based wind farms. International Journal of Ambient Energy, 33(2), 87-97.

[32] He, P., Wen, F., Ledwich, G., & Xue, Y. (2013). Small signal stability analysis of power systems with high penetration of wind power. Journal of Modern Power Systems and Clean Energy, 1(3), 241-248.

Appendices

Abbr/Acro	Description	Unit
v_{ds}	Direct Stator Voltage	p.u.
v_{qs}	Quadrature Stator Voltage	p.u.
i_{ds}	Direct Stator Current	p.u.
i_{qs}	Quadrature Stator Current	p.u.
T_m	Mechanical Torque	s
T_e	Electrical Torque	-
H_m	Rotor Inertia	kWs/kVA
H_t	Wind Turbine Inertia	kWs/kVA
K_s	Shaft stiffness	p.u.
i_{qr}	Quadrature Rotor Current	p.u.
i_{qc}	Quadrature Current	p.u.
i_r	Real Current	p.u.
i_{dr}	Direct Rotor Current	p.u.
i_{dc}	DC Current	p.u.
v_m	Imaginary Voltage	p.u.
I_m	Imaginary Current	p.u.
Ω_b	System Rated Frequency	rad/s
φ	Transformer Phase Shift	-
θ_P	Pitch Angle	rad
x_S	Stator Reactance	p.u.
x_m	Magnetizing Reactance	m/s
K_V	Voltage Control Gain	-
P_{max}	Maximum Active Power	p.u.
P_{min}	Minimum Active Power	p.u.
Q_{max}	Maximum Reactive Power	p.u.
Q_{min}	Minimum Reactive Power	p.u.
T_ϵ	Power Control Time Constant	s
$T_{\epsilon p}$	Active Power Control Time Constant	s
$T_{\epsilon q}$	Reactive Power Control Time Constant	s
δ	Rotor Angle	rad
ω_{mS}	Rotor Angular Speed	p.u.
M	Mechanical starting time (2 * Inertia constant)	kWs/kVA
V_{ref}	Reference Voltage	V
e_r	Real Axis Voltage And Currents Linkage	-
e'_r	Real part of 1st cage voltage	-
e_m	Imaginary Axis Voltage And Currents Linkage	-
e'_m	Imaginary part of 1st cage voltage	-
T_o	Time Integrator Constant	s
ω	angular frequency	Rad/s
p_m	Mechanical Power	w
P^*_w	Power Speed Characteristics	w
b_c	Fixed Capacitor Conductance	p.u.
r_s	Stator Resistance	p.u.
p_e	Electrical Power	w
K_v	Coefficient Of The Voltage Time Derivative	1/s
K_p	Active Px`ower Feedback Gain	gain
T_r	Measurement Time Constant	s
T_p	Pitch Control Time Constant	s
ω_m	Generator Rotor Speed	m/s
γ	Relative angle displacement	p.u.
δ_{SM}	Mechanical Rotor Speed	p.u.
x_d	*d*-axis reactance	p.u.
x_0	Initial Reactance Value	p.u.
x'	1st Reactance Value	p.u.
V_{rmax}	Maximum Regulator Voltage	p.u.
V_{rmin}	Minimum Regulator Voltage	p.u.
K_a	Amplifier Gain	p.u./ p.u.
T_a	Amplifier Time Constant	s
K_f	Stabilizer Gain	p.u./ p.u.
T_f	Stabilizer Time Constant	s
T_v	Voltage Control Time Constant	s
T_e	Field Circuit Time Constant	s
S_e	Ceiling Function Coefficient	-
υ_f	Field Voltage	V
υ^*_f	Feedback Field Voltage	V
ψ_p	Permanent Field Flux	p.u.
x_d	d-axis Synchronous Reactance	p.u.
x'_d	d-axis Transient Reactance	p.u.
e'_q	Constant Amplitude E.M.F.	p.u.
e'_d	Subtransient d-axis Voltage	p.u.
T'_{d0}	d-axis Open Circuit Transient Time Constant	s
T'_{q0}	q-axis Open Circuit Transient Time Constant	s

Table A.1 Abbreviations and Acronyms

Parameter	Value
Stator Resistance (R_s)	0.01
Stator Reactance (X_s)	0.1
Rotor Resistance (R_r)	0.01
Rotor Reactance (X_r)	0.08
Magnetization Reactance (X_m)	3
Inertia Constants (H_m) [kWs/kVA]	3
Number of poles (p)	4
Gear box ratio [int -]	1/89
Pmax [p.u.]	1
Pmin [p.u.]	0
Qmax [p.u.]	0.7
Qmin [p.u.]	-0.7
Pitch control gain (K_p) [p.u.]	10
Time constant (T_p) [s]	3
Voltage Control gain (kv) [p.u.]	10
Power Control time constant (T_e) [s]	0.01
Blade length [m]	75
Blade numbers [int]	3

Table A.2 DFIG Parameters

Parameter	Value
Stator Resistance (Rs)	0.01
Stator Reactance (Xs)	0.1
Rotor Resistance (Rr)	0.01
Rotor Reactance (Xr)	0.08
Magnetization Reactance (Xm)	3
Inertia Constants (Hm) [kVAkWs]	0.05
Inertia Constants Hwr [kWs]	2.5
Inertia Constants Ks [kVA p.u.]	0.3
Number of poles (p)	4
Gear box ratio [int -]	1/89
Blade length [m]	75
Blade numbers [int]	3

Table A.3 SCIG Parameters

Parameter	Value
Stator Resistance (Rs)	0.01
Direct reactances(Xd)	1
Inverse reactances(Xq)	0.8
Constant field flux (Psi_p) [p.u.]	1
Inertia Constants (Hm) [kWs/kVA]	3
Number of poles (p)	4
Gear box ratio [int -]	1/89
Pmax [p.u.]	1
Pmin [p.u.]	1
Qmax [p.u.]	1
Qmin [p.u.]	1
Pitch control gain (K_p) [p.u.]	10
Time constant (T_p) [s]	3
Voltage Control gain (k_v) [p.u.]	10
time constant (T_v) [s]	1
Blade length [m]	75
Blade numbers [int]	3
Active Power Control time constants (T_{eq}) [s]	0.01
Reactive Power Control time constants (T_{eq}) [s]	0.01

Table A.4 PMSG Parameters

Buses	Resistance [p.u.(Ohms/km)]	Reactance [p.u.(H/km)]	Susceptance [p.u.(F/km)]
Bus 7-8	0.0085	0.072	0.149
Bus 7-5	0.032	0.161	0.306
Bus 9-8	0.0119	0.1008	0.209
Bus 9-6	0.039	0.17	0.358
Bus 6-4	0.017	0.092	0.158
Bus 5-4	0.01	0.085	0.176

Table A.5 IEEE 9 Bus Parameters

Bus	Power (S_b^{ac})	Voltage (V_b^{ac})
Bus 1	100	11
Bus 2	100	11
Bus 3	100	11
Bus 4	100	33
Bus 5	100	33
Bus 6	100	33
Bus 7	100	33
Bus 8	100	33
Bus 9	100	33

Table A.6 Base Value

Calculation for Impedance Base

The bases used for ac values for current base and impedance base can be determine using:

- S_b^{ac} three-phase power in MVA.
- V_b^{ac} phase-to-phase voltage in kV.

The current base I_b^{ac} and the impedance base Z_b^{ac} are considered:

- $I_b^{ac} = \frac{S_b^{ac}}{\sqrt{3}.V_b^{ac}}$
- $Z_b^{ac} = \frac{V_b^{ac}}{\sqrt{3}.I_b^{ac}} = \frac{(V_b^{ac})^2}{S_b^{ac}}$

For dc values, the following bases are considered:

- S_b^{dc} power in MW.
- V_b^{dc} voltage in kV.

The current base I_b^{dc} and the resistance base R_b^{dc} are obtained as follows:

- $I_b^{dc} = \frac{S_b^{dc}}{\sqrt{3}.V_b^{dc}}$
- $R_b^{dc} = \frac{V_b^{dc}}{I_b^{dc}} = \frac{(V_b^{dc})^2}{S_b^{dc}}$

Elsewhere, in both ac and dc devices, it is assumed that

- $S_b^{dc} = S_b^{ac}$